DOI: 10.11835/j.issn.2096-6717.2024.045

开放科学(资源服务)标识码OSID:

Calibration of relative density for dense sand using CPTs under high stresses

HAN Feng, WANG Dong, SHI Zhongguo

(Shandong Engineering Research Center of Marine Exploration and Conservation, Ocean University of China, Qingdao 266100, Shandong, P. R. China)

Abstract: Currently, there is a lack of in-situ or model test results for cone penetration tests (CPTs) conducted in deep, dense sand layers under high overburden stresses, restricting the development of empirical relationships between CPT results and the characteristics of such deep, dense sand layers. This study addresses this gap by proposing an empirical relationship to predict the relative density of dense silica sand based on stress level and cone tip resistance. The relationship was developed through CPTs performed in a calibration chamber using dense sand specimens (with relative densities of 74%-91%) subjected to high stresses (under overburden stresses of 0.5-2.0 MPa) and numerical simulations employing the large deformation finite element method. The Arbitrary Lagrangian Eulerian method was used to regularly regenerate the mesh to prevent soil element distortion around the cone tip. Additionally, the modified Mohr-Coulomb model was integrated to capture the stress-strain behavior of dense silica sand under high stresses. A reasonable agreement was achieved between the numerical and experimental penetration profiles, which verifies the reliability of the numerical model. A sufficient number of parametric analyses were carried out, and then an empirical equation was proposed to establish the relationship between the relative density of dense sand, stress level and cone resistance. The empirical equation provides predictions with acceptable accuracy, as the discrepancies between the predicted and measured relative density values fall within ±30%.

Keywords: deep silica sand; dense sand; cone penetration tests; high stresses; calibration chamber; large deformation finite element

高压静力触探试验标定密实砂土的相对密实度

韩锋,王栋,史忠国

(中国海洋大学 海底开发与保护山东省工程研究中心,山东 青岛 266100)

摘　要:高应力水平下深部密实石英砂层中的静力触探原位试验或模型试验数据极少,难以建立静力触探试验结果与深部密实砂层工程性质间的相关性。进行高压标定罐试验,以砂雨法制备相对密实度为74%～91%的密实砂样,在0.5～2.0 MPa的高应力水平下开展标定罐中的静力触探试验。采用修正摩尔库伦本构模型描述高应力水平下密实石英砂的应力-应变响应,并纳入任意拉格朗日-欧拉大变形有限元方法,对静力触探试验进行数值模拟。这种大变形方法能有效避免锥尖周围土体网格的严重扭曲,保证计算收敛。数值模拟与标定罐试验结果基本吻合,证明了大变形分析的可靠性。总结试验和数值数据发现,锥尖贯入阻力是砂土相对密实度和所处应力水平的函

Received: 2024-04-20

Foundation items: National Natural Science Foundation of China (Nos. 42025702, 52394251)

Author brief: HAN Feng (1999-), main research interest: offshore geotechnical engineering, E-mail: hanfeng@stu.ouc.edu.cn.

WANG Dong (corresponding author), professor, doctorial supervisor, E-mail: dongwang@ouc.edu.cn.

数，且仍可采用低应力水平下函数表达的基本形式。进行充分数量的变动参数分析，拟合得到高应力水平下密实石英砂相对密实度预测公式中的参数，将公式预测结果与标定罐试验结果对比，发现预测效果较好，相对误差小于30%。

关键词：深部石英砂；密实砂土；静力触探；高应力水平；标定罐；大变形有限元

中图分类号：TU411.93　　**文献标志码**：A　　**文章编号**：2096-6717(2025)06-0106-08

1 Introduction

Dense or very dense sand layers formed under high stresses frequently occur in onshore and offshore practices. For example, the piles supporting high-rise buildings and nearshore fixed platforms are driven to depths exceeding 60 m or even deeper than 100 m[1-3]. The relative densities of deep sand layers near the piles were typically larger than 60%, with the overburden stresses (effective stress) of at least 0.5 MPa[1-2]. Another example is that in the second natural gas hydrate production test in the eastern Nankai Trough, the production wells were inserted into the sandy reservoir layer at depths ranging from 275.8 m to 337.3 m underneath the seabed surface. This sandy layer is subjected to vertical effective stresses of approximately 1.5 MPa, with relative densities reported to be greater than 70%[3].

It is hard to obtain high-quality samples of silica sands in most geological investigations. Therefore, due to its cost-effectiveness and rapid characterizations, the in-situ cone penetration test (CPT) has been used widely to determine soil properties[4-5]. For CPT tests, a large number of chamber tests, in-situ measurements, and numerical studies have been conducted during the last five decades to obtain the relative density, internal friction angle, and over-consolidation ratio of sand through the cone tip resistance measured[4-6], and several empirical relationships between the relative density, overburden stress, and tip resistance have been proposed[7-10]. Conventionally, most of the studies were conducted under overburden stresses below 0.5 MPa. Most recently, Kong et al. [11] conducted chamber tests of CPT with overburden stresses ranging between 0.5-2.0 MPa. However, the relative densities of their sand specimens were limited to 45.2%-62.1% due to limitations on specimen preparation. Furthermore, several sand types in practical applications are beyond the upper limit of their range[1-3].

In addition to model tests conducted in the calibration chamber, finite element methods are widely employed to elucidate the mechanisms of CPTs in sand[12-14]. To mitigate excessive mesh distortion during penetration, the Arbitrary Lagrangian Eulerian (ALE) approach, integrated within the commercial package Abaqus, has been significantly advanced[15]. The ALE is an r-adaptive method, which conducts frequent mesh generations near the penetrometer[15-16]. Notably, it preserves the mesh topology and allows the mesh to move independently of the material to eliminate possible mesh distortion[16]. During this process, a combination of Lagrangian and Eulerian steps is used.

In this paper, CPTs in a calibration chamber and numerical simulations using the ALE method were conducted for deep, dense sand layers with overburden stresses greater than 0.5 MPa and relative densities exceeding 65% to establish an empirical relationship between the relative density, overburden stress, and tip resistance. A modified Mohr-Coulomb (MMC) constitutive model, similar to the models used by Mohammadi et al. [17] and Hu et al. [18], was adopted in numerical simulations to describe the stress-strain relationship of the silica sand.

2 Arrangement of tests

2.1 Equipment

The Ocean University of China developed the calibration chamber used in this study. It is a double-wall chamber designed to accommodate a cylindrical soil specimen with dimensions of 600 mm in diameter and 750 mm in height. A membrane made of natural and abrasion-resistant rubber enclosing the soil specimen was used in this chamber to independently control the axially symmetric lateral pressure, which was applied by water pressure. Vertical pressure was applied by a hydraulic cylinder connected to the base of the specimen. The maximum cell pressure used in the calibration chamber does not exceed 5 MPa. Various control and measurement devices are integrated into the calibration chamber to monitor the lateral

pressure, vertical pressure, and specimen base displacement.

In the chamber, a cone with a diameter of D= 20 mm and an apex angle of 60° penetrated the sand at a constant rate of 20 mm/s.

2.2 Preparation of specimens and testing conditions

During this study, reconstituted fine Qingdao silica sand specimens were prepared and tested in the calibration chamber. The specific gravity of particles in the sand was 2.65, with a mean particle size D_{50} of 0.173 mm and a coefficient of uniformity of 1.70. The Poisson's ratio υ was taken as an empirical value of 0.35. The particle size distribution is presented in Fig. 1. The maximum and minimum void ratios for the sand are e_{max}=0.949 and e_{min}=0.490, respectively.

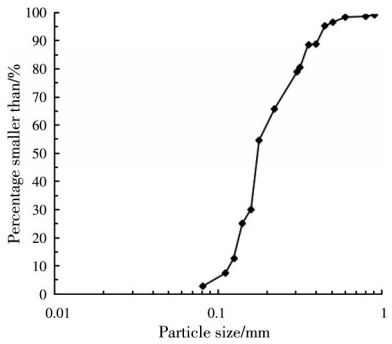

Fig. 1 Particle size distribution of Qingdao sand

Typically, the sand around the conical probe is involved under drained conditions. According to the findings reported by Kluger et al. [19], there is no significant disparity in tip resistance between dry and saturated sand specimens when the confining stress exceeds 0.2 MPa. Therefore, dry silica sand specimens were used in this study to save testing efforts.

The reconstituted sand specimens were prepared using the pluvial deposition technique. The sand was placed in a gravity mass sand spreader positioned above the chamber, as shown in Fig. 2. The opening size of the spreader and the drop height of the sand influence the relative density (D_r, in the absence of further specification, throughout this paper, relative densities mentioned refer to those obtained after consolidation) of the specimens significantly. To prepare specimens with D_r of 74.1%-77.4% and 80.7%-90.9%, the opening sizes of the spreader were set at 2 mm and 1 mm, respectively, with a sand drop height of 1 300 mm for both cases. During the specimen preparation process, once the surface of the sand specimen reached the markings made at intervals of 0.1 m inside the calibration chamber, the sand spreader was raised by 0.1 m to ensure that the drop height of the sand remained constant.

Fig. 2 Sand spreader mounted on the top of the chamber

CPTs were performed on dense silica sand specimens reconstituted to different D_r and consolidated under three confining pressures σ'_v (0.5, 1.0, 2.0 MPa, each applied isotropically). Four cutting rings with bases were used to measure the D_r of each specimen. Each cutting ring has a volume of 200 cm^3 and was placed at the bottom of the chamber. The steady cone tip resistance q_c approaches at the penetration depth of around 10D. The results of CPTs in the calibration chamber are presented in Table 1.

Table 1 Measured tip resistances in the chamber

D_r/%	e	σ'_v/MPa	q_c measured/MPa
74.1	0.609	1.0	43.7
77.4	0.594	2.0	52.0
82.3	0.571	0.5	28.8
80.7	0.579	1.0	46.7
82.3	0.571	0.5	35.1
80.7	0.579	1.0	50.7
90.9	0.532	2.0	64.9

3 Numerical analysis

3.1 Soil model and material properties

The classic Mohr-Coulomb model specifies the internal friction angles and dilation angles as fixed values; thereby, it cannot account for the effect of strain-softening and dilatancy. To overcome the limitation, a modified Mohr-Coulomb model was developed by Hu et al. [18] has been incorporated into the numerical analysis. The MMC model makes the internal friction angle φ and dilation angle ψ as dependent variables of the accumulated plastic shear strain γ. The

relation is shown schematically in Fig. 3, where the internal friction angle increases linearly from the initial value, φ_i, to the peak value φ_p and then reduces linearly to the critical value φ_{cv}, which means reaching the critical state. As for the dilation angle, it remains 0 when $\gamma < \gamma_1$ because the Mohr-Coulomb model cannot converge with a negative dilation angle. The dilation angle also increases linearly to the peak value ψ_p before the accumulated plastic shear strain reaches γ_2 and then remains at ψ_p until γ_3. Additionally, the dilation angle reduces linearly when $\gamma_3 < \gamma < \gamma_4$, and finally returns to 0 at the critical state. Notably, the strain-hardening or strain-softening behavior during shearing depends on the sand's relative density and stress level. The MMC model degenerates to the traditional Mohr-Coulomb model when sand specimens are contractile and strain-hardening. This means the internal friction angle remains at $\varphi_{cv,}$ and the dilation angle remains at 0. By following Hu et al. [18] and Zheng et al. [20], φ_i was specified as the same as φ_{cv}, γ_1, γ_2, γ_3 and γ_4 were taken as 1.0%, 1.2%, 5.0% and 15.0%.

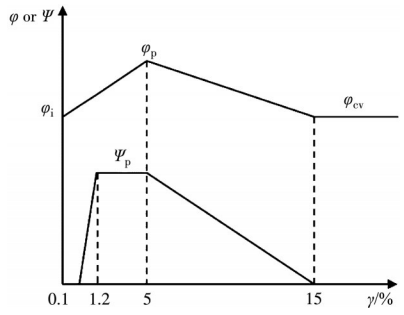

Fig. 3　Variations of internal friction and dilation angles of the MMC model

The bender element tests were performed in a triaxial apparatus to determine the maximum elastic shear modulus G_{max} under a small strain level of 10^{-6}. After each time the specimen was consolidated under the mean effective stress p', the void ratio e and G_{max} were obtained by determining the volume change and bender element tests, respectively. G_{max} can be seen as a function of e and p'[21]. In this study, we adopted the correlation proposed by Chow et al. [22], as depicted in Equation (1), P_a is the atmospheric pressure, and the parameters were empirically fitted to C_1=800, C_2=1.95 and C_3=0.7. The bender element test results are presented in Table 2.

$$G_{max} = C_1 \frac{(C_2 - e)^2}{1 + e} \left(\frac{p'}{P_a} \right)^{C_3} P_a \tag{1}$$

Table 2　Bender element test results

e	p'/MPa	G_{max}/MPa
0.627	0.1	119.6
0.620	0.2	175.8
0.615	0.3	222.2
0.610	0.4	263.2
0.607	0.5	301.1
0.600	0.7	370.5
0.593	1.0	459.5
0.590	1.2	515.7
0.584	1.5	592.7
0.597	0.1	126.7
0.591	0.2	186.4
0.585	0.3	235.6
0.581	0.4	279.0
0.577	0.5	319.2
0.570	0.7	392.7
0.564	1.0	487.1
0.561	1.2	547.6
0.556	1.5	629.4

The elastic shear modulus G of the MMC model is under a strain level of 10^{-2}. Following the approach proposed by Loukidis et al. [23], the elastic shear modulus in the MMC model was obtained through $G = G_{max}/T$. According to the method recommended by Papadimitriou et al. [24] and Pei et al. [25], T was taken as 4.3 for CPTs in sand.

Drained triaxial tests were carried out to determine the φ and ψ. A shearing rate of 0.5%/min was adopted for all tests. φ_p and φ_{cv} can be obtained according to specimens' peak strength and critical strength, respectively. φ_{cv} was taken as 33.8°, which agrees with triaxial test results. The peak slope of the curve showing the change in sand specimen volume strain with axial strain can be used to obtain the value of ψ_p. Referring to the form of the original Bolton formula as Equation (2)-Equation (4)[26], the parameters were empirically fitted to m=3.2 and k=1.3. I_R is the coefficient of dilatancy.

$$I_R = D_r(10 - \ln p') - 1 \tag{2}$$

$$\varphi_p - \varphi_{cv} = mI_R \tag{3}$$

$$\psi_p = k(\varphi_p - \varphi_{cv}) \tag{4}$$

3.2　Finite element modeling

ALE, a large deformation finite element approach with explicit integration schemes in the com-

mercial package Abaqus[15], was used to mimic the cone penetration tests. We simplified the cone penetration into sand as an axis-symmetric boundary value problem. The ALE model of CPT is shown in Fig. 4. It is essential to ensure the effectiveness of mesh moving to eliminate possible mesh distortions when the calculation results are not affected; as a solution, a smooth rigid tube that moved together with the cone was set between the cone and soil by following Fan et al. [27]. In doing so, we let the leftmost soil elements move outwards to the axis of symmetry instead of inwards.

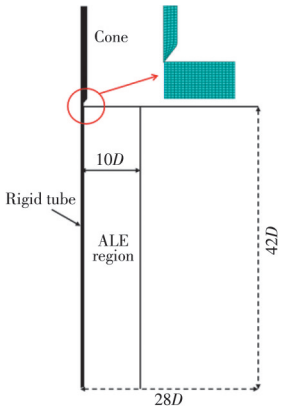

Fig. 4 ALE model of CPT

For the two-dimensional axisymmetric calculation, the width and height of the soil domain are $28D$ and $42D$, respectively, while D represents the cone diameter and is 20 mm. The dimensions of the soil domain have been proven to be sufficiently large to avoid boundary effects. To reduce the computational load, an ALE region with a width of $10D$ is implemented for mesh adjustment. Based on preliminary calculations, the element size within the ALE region is set to $D/8$. The mesh quality in the ALE region must also be maintained after node position adjustments to avoid distortion. For this purpose, the built-in geometric enhancement form of the mesh smoothing method in Abaqus is employed.

The penetration velocity of the cone was set to 20 mm/s, which was sufficiently slow to ensure a quasi-static analysis. The lateral earth pressure coefficient K_0 was set to 1 to facilitate a comparison with calibration chamber tests. The hard contact algorithm was also employed to simulate the interaction between the penetrometer and the soil. Given that the lateral frictional resistance on the penetrometer in sand is significantly smaller than the tip resistance, the frictional stress at the interface between the cone and sand was set to 0.

4 Verification

Fig. 5 compares the tip resistance results from numerical simulations and calibration chamber tests. The relative densities corresponding to each curve can be determined through Table 1. It can be observed from the calibration chamber test results that each tip resistance curve can be divided into three distinct stages. In the first stage, where the penetration depth varies from 0 to $1.5D$, the tip resistance grows nearly linearly with the depth. This growth rate is also positively associated with both the σ_v' and the D_r of the sand specimen. The second stage occurs between the penetration depth of $1.5D$ and $10D$, during which the slope of increase in the tip resistance decreases, and the value of the tip resistance demonstrates a progression towards stabilization as the penetration depth increases. Finally, the tip resistance maintains a substantially stable condition in the third stage, where the penetration depth surpasses $10D$.

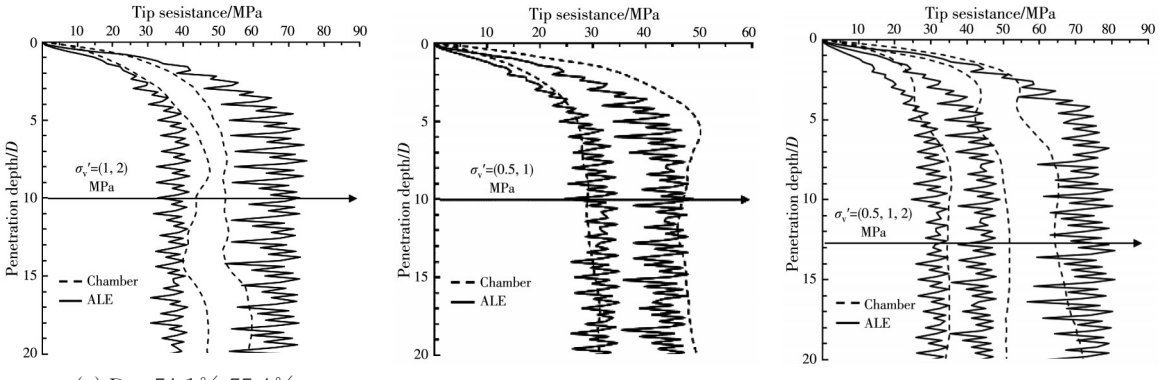

(a) D_r=74.1%-77.4% (b) D_r=80.7%-82.3% (c) D_r=80.7%-90.9%

Fig. 5 Comparison of calibration chamber and ALE results

Under high stresses, the q_c continues to increase with higher values of D_r and σ_v' in sand specimens. Comparing the results from calibration chamber tests on specimens with D_r of 74.1%-77.4%, the q_c value at σ_v' of 2 MPa is approximately 1.19 times higher than that at σ_v' of 1 MPa. Meanwhile, for specimens with D_r of 80.7%-90.9%, the q_c values at σ_v' of 1 MPa and 2 MPa are approximately 1.44 and 1.85 times higher than that at σ_v' of 0.5 MPa. This indicates that, under high stresses, q_c remains dependent on the confining pressure. Under equivalent σ_v', the q_c values of sand specimens with D_r of 80.7%-90.9% are found to be within the range of 1.16 to 1.25 times higher than the q_c values of specimens with D_r of 74.1%-77.4%. Thus, under high stresses, q_c remains dependent on the relative density.

Generally, a reasonable agreement was achieved between the numerical and calibration chamber test results. These findings indicate that the MMC model and the ALE method effectively simulate the cone penetration test process in dense silica sands under high stresses. From the results, it can be observed that:

(1) When the penetration depth exceeds $10D$, the numerical tip resistance results remain relatively stable, with any fluctuations in the data attributed to an acceptable noise level.

(2) q_c exhibits significant similarity between the results obtained from calibration chamber tests and numerical simulations. The tip resistance results from the two methods exhibit close agreement for sand specimens with σ_v' of 0.5 MPa and 1 MPa. For sand specimens with σ_v' of 2 MPa, the q_c values from numerical simulations for sand specimens with D_r of 77.4% and 90.9% are approximately 26.1% and 11.1% greater than the q_c values from calibration chamber tests, respectively.

5 Estimating D_r based on q_c and σ_v'

A parametric analysis was conducted to establish a quantitative relationship between the q_c, σ_v', and D_r for dense silica sands under high overburden stresses; the numerical results are presented in Table 3. G_{max} was determined using Equation (1), while the φ_p and ψ_p were calculated based on Equations (2)-Equations (4).

Table 3　ALE numerical results

D_r/%	σ_v'/MPa	q_c/MPa
65	0.5	25.8
	0.8	34.5
	1.0	40.8
	1.3	46.5
	1.6	54.4
	2.0	58.9
75	0.5	29.0
	0.8	39.3
	1.0	44.0
	1.3	51.9
	1.6	61.8
	2.0	64.5
85	0.5	30.7
	0.8	42.7
	1.0	49.9
	1.3	59.3
	1.6	67.5
	2.0	73.8
95	0.5	36.0
	0.8	49.4
	1.0	53.9
	1.3	69.1
	1.6	74.6
	2.0	75.5

Upon comparing the results at D_r of 65% and 85%, it was observed that under the same σ_v', the q_c value at D_r of 85% is approximately 1.24 times greater than that at D_r of 65%. When considering different values of σ_v', the q_c values under σ_v' of 0.8 MPa, 1.0 MPa, 1.3 MPa, 1.6 MPa, and 2.0 MPa were found to be 1.36 times, 1.6 times, 1.87 times, 2.15 times and 2.34 times greater than those under σ_v' of 0.5 MPa, respectively.

Upon synthesizing the numerical results across all 24 distinct conditions, it was observed that the empirical correlation proposed by Lunne et al. in equation (5) for predicting D_r based on q_c and σ_v' remains valid under high overburden stresses ranging from σ_v' =0.5 MPa to 2 MPa[7]. Notably, this correlation was initially developed based on CPT results conducted on silica sands with overburden stresses less than 0.5 MPa. In the context of dense silica sand under high overburden stresses, the empirical fitting of equation (5) resulted in the following parameter values: k_1=0.737, n=0.582, and k_2=2.74.

$$D_r = k_1 \ln\left[\left(\frac{q_c}{P_a}\right)\Big/\left(\frac{\sigma_v'}{P_a}\right)^n\right] - k_2 \quad (5)$$

According to Equation (5), the predicted values of D_r were calculated based on the measured values obtained from calibration chamber tests conducted on dense sand specimens subjected to high stresses in this study. These results are illustrated in Fig. 6, including the model test results from Lunne et al. [7], Pournaghiazar et al. [8], Sadrekarimi et al. [10], Kluger et al. [19], Bolton et al. [28] and Kong et al. [11]. The test results from the first five studies were obtained under low overburden stresses. In contrast, those from Kong et al. were obtained under high overburden stresses. The types of sand used in the six studies were fine to medium Ticino sand[7], Sydney sand[8], Fraser River sand[10], medium-coarse to coarse Ticino sand[19], fine Fontainebleau sand[28], and fine Qingdao sand[11].

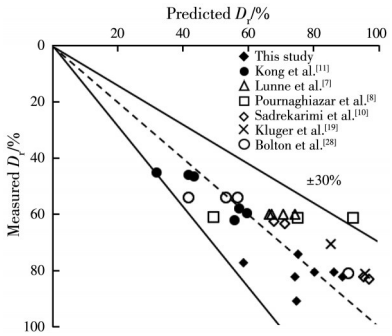

Fig. 6 Relative densities measured and predicted by Equation (5)

A reasonable agreement was achieved between the predicted and measured D_r. Equation (5) effectively predicts the D_r of sand specimens under high and low overburden stresses. Moreover, discrepancies between the predicted and measured values fall within the range of ±30%.

6 Conclusion

Cone penetration tests were conducted in a calibration chamber using dense sand specimens under high stresses in conjunction with a numerical study employing the ALE method. The results of the calibration chamber tests and numerical simulations demonstrate reasonable agreement, providing the following key findings:

(1) Based on the numerical results obtained from dense sand specimens under high overburden stresses, an empirical relationship has been established for predicting D_r using q_c and σ_v'. A limitation of this study is that only the case where $K_0=1$ was considered.

(2) The empirical relationship shows satisfactory predictive performance for specimens under high and low overburden stresses, with the relative density predictions deviating within ±30% of the measured values.

References

[1] ELSAYED T, EL-SHAIB M, GBR K. Reliability of fixed offshore jacket platform against earthquake collapse [J]. Ships and Offshore Structures, 2016, 11(2): 167-181.

[2] COMODROMOS E M, RANDOLPH M F. Improved relationships for the pile base response in sandy soils [J]. Journal of Geotechnical and Geoenvironmental Engineering, 2023, 149(8): 04023058.

[3] FUJII T, SUZUKI K, TAKAYAMA T, et al. Geological setting and characterization of a methane hydrate reservoir distributed at the first offshore production test site on the Daini-Atsumi Knoll in the eastern Nankai Trough, Japan [J]. Marine and Petroleum Geology, 2015, 66: 310-322.

[4] LEE J, EUN J, LEE K, et al. In-situ evaluation of strength and dilatancy of sands based on CPT results [J]. Soils and Foundations, 2008, 48(2): 255-265.

[5] KROGH L, QUINTEROS S, ENGIN H K, et al. Revisiting interpretation of relative density from shallow depth CPTs in sand [J]. Canadian Geotechnical Journal, 2022, 59(6): 808-826.

[6] MARTINELLI M, GALAVI V. Investigation of the material point method in the simulation of cone penetration tests in dry sand [J]. Computers and Geotechnics, 2021, 130: 103923.

[7] LUNNE T, POWELL J J M, ROBERTSON P K. Cone penetration testing in geotechnical practice[M]. RC Press, 2002.

[8] POURNAGHIAZAR M, RUSSELL A R, KHALILI N. The cone penetration test in unsaturated sands [J]. Géotechnique, 2013, 63(14): 1209-1220.

[9] GHALI M, CHEKIRED M, KARRAY M. A laboratory-based study correlating cone penetration test resistance to the physical parameters of uncemented sand mixtures and granular soils [J]. Engineering Geology, 2019, 255: 11-25.

[10] SADREKARIMI A, JONES S. Laboratory-scale seismic CPT calibration chamber tests on Fraser River sand [J]. Canadian Geotechnical Journal, 2022, 59(8): 1386-1400.

[11] KONG Z Z, WANG D, ZHANG M S, et al. High-pressure cone penetration tests in silica sand using calibration chamber and large deformation analysis [J]. Journal of Civil and Environmental Engineering, 2023, 45(4): 49-55. (in Chinese)

[12] JARAST P, GHAYOOMI M. Numerical modeling of cone penetration test in unsaturated sand inside a calibration chamber [J]. International Journal of Geomechanics, 2018, 18(2): 04017148.

[13] CHEN Z Q, HUANG M S, SHI Z H. Application of a state-dependent sand model in simulating the cone penetration tests [J]. Computers and Geotechnics, 2020, 127: 103780.

[14] PEI H M, WANG D, LIU Q B. Numerical study of relationships between the cone resistances and footing bearing capacities in silica and calcareous sands [J]. Computers and Geotechnics, 2023, 155: 105220.

[15] ABAQUS Inc. ABAQUS analysis user's manual. Version 6.14 [Z]. Providence, RI: Dassault Systèmes, 2014.

[16] WANG D, BIENEN B, NAZEM M, et al. Large deformation finite element analyses in geotechnical engineering [J]. Computers and Geotechnics, 2015, 65: 104-114.

[17] MOHAMMADI S, TAIEBAT H A. A large deformation analysis for the assessment of failure induced deformations of slopes in strain softening materials [J]. Computers and Geotechnics, 2013, 49: 279-288.

[18] HU P, WANG D, STANIER S A, et al. Assessing the punch-through hazard of a spudcan on sand overlying clay [J]. Géotechnique, 2015, 65(11): 883-896.

[19] KLUGER M O, KREITER S, STÄHLER F T, et al. Cone penetration tests in dry and saturated Ticino sand [J]. Bulletin of Engineering Geology and the Environment, 2021, 80(5): 4079-4088.

[20] ZHENG J, HOSSAIN M S, WANG D. Numerical investigation of spudcan penetration in multi-layer deposits with an interbedded sand layer [J]. Géotechnique, 2017, 67(12): 1050-1066.

[21] OZTOPRAK S, BOLTON M D. Stiffness of sands through a laboratory test database [J]. Géotechnique, 2013, 63(1): 54-70.

[22] CHOW S H, DIAMBRA A, O'LOUGHLIN C D, et al. Consolidation effects on monotonic and cyclic capacity of plate anchors in sand [J]. Géotechnique, 2020, 70 (8): 720-731.

[23] LOUKIDIS D, SALGADO R. Modeling sand response using two-surface plasticity [J]. Computers and Geotechnics, 2009, 36(1): 166-186.

[24] PAPADIMITRIOU A G, BOUCKOVALAS G D, DAFALIAS Y F. Plasticity model for sand under small and large cyclic strains [J]. Journal of Geotechnical and Geoenvironmental Engineering, 2001, 127(11): 973-983.

[25] PEI H M, WANG D, LIU Q B. Large deformation finite element analysis of cone penetration tests in calcareous sands [J]. Journal of Civil and Environmental Engineering, 2021, 43(1): 48-53.

[26] BOLTON M D. The strength and dilatancy of sands [J]. Géotechnique, 1986, 36(1): 65-78.

[27] FAN S, BIENEN B, RANDOLPH M F. Stability and efficiency studies in the numerical simulation of cone penetration in sand [J]. Géotechnique Letters, 2018, 8 (1): 13-18.

[28] BOLTON M D, GUI M W, GARNIER J, et al. Centrifuge cone penetration tests in sand [J]. Géotechnique, 1999, 49(4): 543-552.

(编辑　胡英奎)